Available online at www.sciencedirect.com
ScienceDirect
Trans. Nonferrous Met. Soc. China 31(2021) 3752−3761
Transactions of Nonferrous Metals Society of China
www.tnmsc.cn

Experiment and modeling of TiB_2/TiB boride layer of Ti−6Al−2Zr−1Mo−1V alloy

De-lai OUYANG[1], Sheng-wei HU[1], Cheng TAO[1], Xia CUI[1], Zhi-shou ZHU[2], Shi-qiang LU[1]

1. Key Laboratory for Microstructural Control of Metallic Materials of Jiangxi Province, Nanchang Hangkong University, Nanchang 330063, China;
2. Beijing Institute of Aeronautical Materials, Beijing 100095, China

Received 30 March 2021; accepted 21 October 2021

Abstract: The influence of the boriding conditions on the boride layers was examined by boriding Ti−6Al−2Zr−1Mo−1V alloy in the temperature range of 920−1120 °C. The experimental results show that the boride layers were composed of a continuous thin outer layer of TiB_2 and a thick inner layer of TiB with whiskers or needle-like morphologies that extended into the substrate. Thick and compact boride layers were obtained when the boriding temperatures were 1000−1080 °C, and the treatment time exceeded 8 h. The boride layer depth increased with the boriding temperature and time, and the growth kinetics of the boride layers was characterized by a parabolic curve. The growth kinetics of the boride layers, including both TiB_2 and TiB layers, were predicted by establishing a diffusion model, which presented satisfactory consistency with the experimental data. As a result, the activation energies of boron in the TiB_2 and TiB layers were estimated to be 223.1 and 246.9 kJ/mol, respectively.
Key words: Ti−6Al−2Zr−1Mo−1V alloy; boriding; microstructure; modeling

1 Introduction

Due to medium strength at room temperature and high temperature, good thermal stability, creep resistance and corrosion resistance [1,2], Ti−6Al−2Zr−1Mo−1V alloy has been widely used in important structural parts with complex designs, especially in aeronautical aircraft partition frames and ribbed panels [3,4]. However, Ti−6Al−2Zr−1Mo−1V alloy has low surface hardness and poor wear resistance, which limits its applications as wear parts in certain mechanical structures (such as micro-disturbance wear and small- and medium-load gears). Thus, surface modification is required to improve its wear resistance and extend its service life [5].

Boriding, as a thermochemical surface treatment, is an effective surface-hardening process that has been primarily applied in steels [6] and nickel alloys [7]. Due to good hardness and tribological properties of titanium boron compounds, boriding in titanium and its alloys has been widely studied in recent years [8]. Because boron atoms diffuse into the substrate during the thermochemical surface treatment process, boriding forms hard boride layers on the surface and can improve the hardness and wear resistance of titanium and its alloys [9]. Boriding is usually performed in the temperature range of 900−1000 °C by pack-boriding, molten salt-boriding and paste-boriding methods. Generally, dual boride layers of TiB_2 and TiB can be obtained. SARMA et al [10] created boride layers that are composed of a monolithic titanium diboride (TiB_2) layer at the top and a titanium boride (TiB) sublayer by solid-state boron

Corresponding author: Zhi-shou ZHU, Tel: +86-797-83863039, E-mail: zhuzzs@126.com; Xia CUI, E-mail: cuixia2000@163.com
DOI: 10.1016/S1003-6326(21)65761-8

diffusion through the titanium surface. LI et al [11] showed dual boride layers with an outer TiB_2 layer and an inner TiB layer formed on the surface of a borided TB_2 alloy by pack boriding in the temperature range of 950−1100 °C. The micro-hardness and coefficients of friction of borided layers can reach ~27.5 GPa and ~0.35, respectively. In addition, the borided layer has excellent adhesion to the substrate due to the nature of the thermal diffusion process. This adhesion plays an important role in improving the wear resistance and promoting the application of boriding for titanium and its alloys. To achieve the optimal boride layers and promote the application of boriding for Ti alloys, it is necessary and significant to develop a growth model of borided layers to predict the boride layer thickness.

A few attempts have been reported to model the growth kinetics of boride layers in the pack-boriding process. KEDDAM and TAKTAK [12] proposed a diffusion model to estimate the diffusion coefficient of boron in the TiB_2 and TiB layers of Ti6Al4V alloy. This model was based on solving the mass balance equations at two (TiB_2/TiB and TiB/Ti) interfaces by considering the effect of boride incubation time during the formation of TiB_2 and TiB layers. Additionally, KARA and PURCEK [13] verified that the diffusion model was applicable for predicting the boride layer growth kinetics of a β-type Ti−45Nb alloy. LIU et al [14] suggested that the growth kinetics of these dual boride layers of Ti−5Mo−5V−8Cr−3Al alloy (TB_2 alloy) during pack boriding with CeO_2 obeyed the diffusion model of $d=kt^{0.5}$ instead of $d^2=Dt$. To date, although these models present satisfactory consistency between the predictions of the boride layer thickness and the experimental data [15,16], limited studies have been performed on modeling the growth kinetics of the boride layers formed on Ti−6Al−2Zr−1Mo−1V alloys. Thus, it is necessary to examine the growth kinetics of TiB_2/TiB layers and predict the boride layer thickness of Ti alloys.

This study aimed to fully investigate the growth kinetics and estimate the boride layer thickness, including TiB_2 and TiB layers, of Ti−6Al−2Zr−1Mo−1V alloy during the pack-boriding process in the temperature range of 920−1120 °C. For this purpose, the influences of boriding parameters (mainly temperature and time) on the borided layer were examined. A diffusion model was established based on the boron concentration profiles of the surface layers, parabolic growth law, and mass balance equations of the TiB_2/TiB and TiB/substrate interfaces. It also provides an approach to predict the growth kinetics of the boride layer of titanium and its alloys.

2 Experimental

Ti−6Al−2Zr−1Mo−1V alloy was chosen as the substrate material to be boronized. The alloy samples were cut into specimens with sizes of 12 mm × 12 mm × 15 mm by a wire cutting machine. Prior to boronizing, the specimen surfaces were ground using emery paper, polished using a polishing cloth to remove the oxide layers and irregularities and ultrasonically cleaned in acetone for 20 min. Then, they were packed with a powder mixture of 35 wt.% B_4C, 64 wt.% SiC and 1 wt.% Al in a sealing stainless steel container with clay and borided in the temperature range of 920−1120 °C for 5−20 h in a vacuum furnace at a pressure of 1×10^{-5} Pa. Oxidation during boriding can be prevented under such vacuum conditions. The boriding temperatures of 920−1120 °C were selected because TiB whiskers grow fast when the boriding temperature is approximately the β-phase transition temperature of 980 °C. Once the treatments were completed, the container was removed from the vacuum furnace and cooled to room temperature in air.

After boronizing, the samples for metallographic examination were taken from the cross section of boronizing workpieces. The samples were polished to a 1200 grit surface finish and cleaned with distilled water followed by acetone. The microstructures of the borided layers were observed using an XJP-6H optical microscope with a built-in quantitative analysis system. The thickness of the boride layers was determined as the average of 12 measurements. Since the boride layers show features of protrusions, the thickness measurements should be conducted carefully, as shown in Fig. 1. SEM image analysis was performed on a JEM−200CX scanning electron microscope. The phase analysis was performed on a D8 X-ray diffractometer.

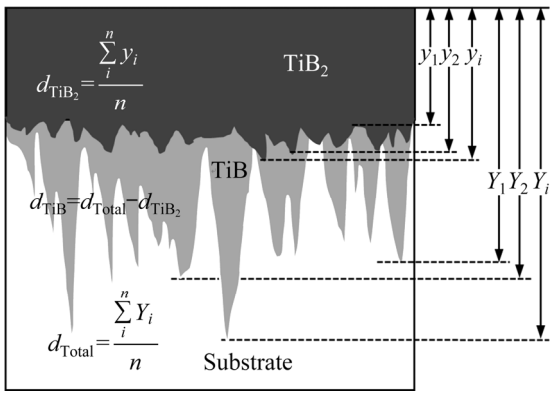

Fig. 1 Schematic representation of measurement of borided layer thickness

3 Results and discussion

3.1 Structure of boride layers

Figure 2 shows the typical characteristics of the boride layers of Ti−6Al−2Zr−1Mo−1V alloy. The cross-sectional SEM micrographs of the boride layers reveal the dual layers of TiB_2 and TiB. A continuous thin outer layer of TiB_2 and a thick inner layer of TiB with whiskers or a needle-like morphology, which extended into the substrate, were observed. This characteristic of the boride layers was reported in other titanium alloys by several researchers, such as in Ti6Al4V alloy by PENG et al [17], in pure titanium by LV et al [18], and in TiAl intermetallics by POPELA and VOJTĚCH [19]. In addition, it is easy to observe that there were no microcracks or holes at the TiB_2/TiB and TiB/Ti interfaces; thus, tight bonding between the boride layers and the substrate was expected. The different morphologies between TiB_2 and TiB layers may be attributed to different preferential directions of crystal growth of TiB_2 and TiB [20]. Generally, TiB_2 and TiB are considered to have hexagonal and orthorhombic structures, respectively. The preferential growth direction in TiB_2 is [1100] and it will grow as a graphite-like boron layer perpendicular to [0001] direction. The preferential growth direction in TiB is [010], where three types of specific orientation relationships between TiB and β-Ti are as follows [18]: $[010]_{TiB}$// $[010]_{\beta\text{-Ti}}$, $[010]_{TiB}$//$[001]_{\beta\text{-Ti}}$, and $[010]_{TiB}$//$[111]_{\beta\text{-Ti}}$. As a result, TiB will grow as a needle-like or whisker-like morphology along [010] direction.

Figure 3 shows cross-sectional micrographs of the boride layer of Ti−6Al−2Zr−1Mo−1V alloy borided at 1040 °C for different time. The observed combined TiB_2 and TiB thickness of the alloy increased with increasing treatment time. The XRD analysis in Fig. 4 provides evidence for the existence of TiB_2 and TiB phases.

At 1040 °C and a treatment time of no longer than 8 h (Figs. 3(a, b)), relatively thin TiB_2 and TiB layers were visible, which resulted in an unobvious TiB_2 layer. When the treatment time increased to 12 h, a continuous TiB_2 layer with a thickness of approximately 3.6 μm was observed (Fig. 3(c)). Much thicker and compact boride layers were obtained after 15 and 18 h (Figs. 3(d, e)), where the boride layer thicknesses were 27 and 29 μm, respectively. When the treatment time increased to 20 h, 31 μm-thick boride layer was obtained.

The influences of the temperature for a given treatment time of 20 h on the microstructure associated with the boride layers are illustrated in Fig. 5. Under different heating temperature

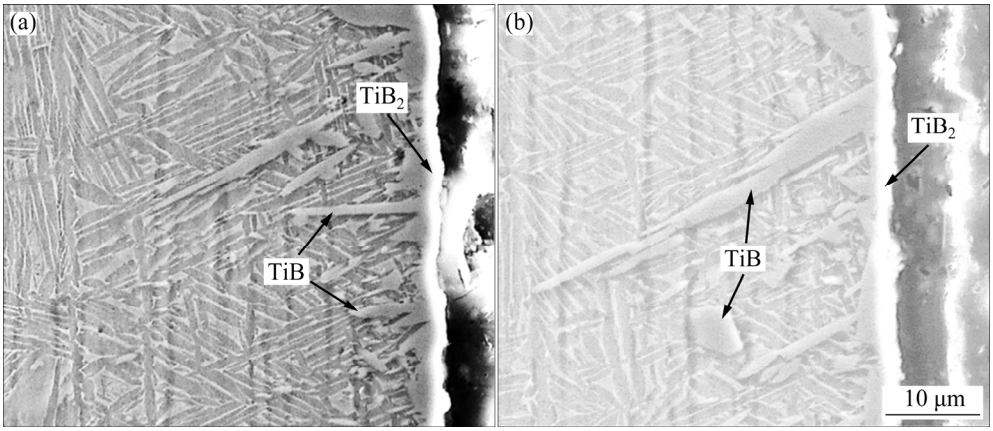

Fig. 2 SEM micrographs of coating structure in Ti−6Al−2Zr−1Mo−1V alloy borided at 1040 °C for 10 h (a) and 20 h (b)

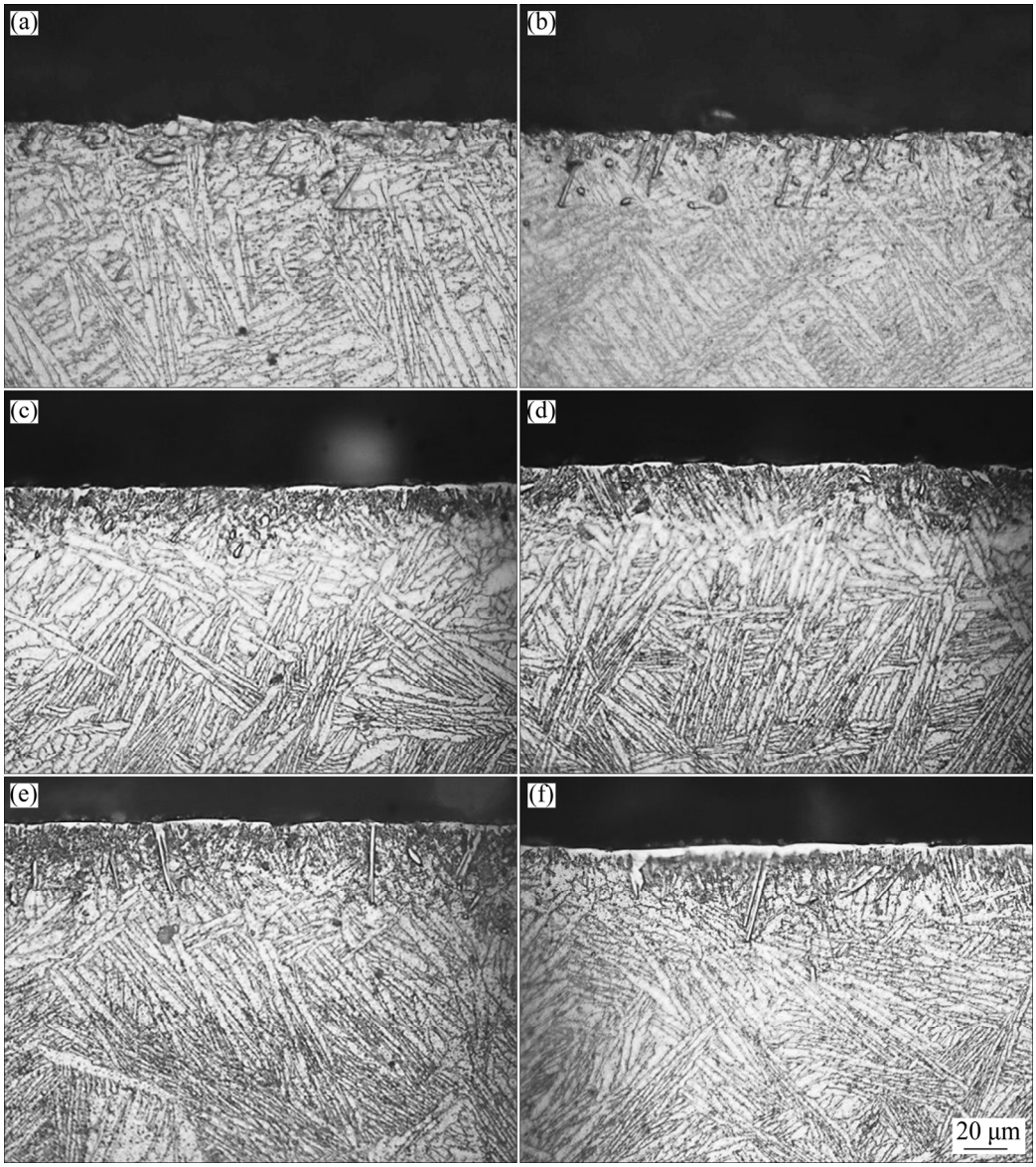

Fig. 3 Cross-sectional micrographs of boride layer of alloy borided at 1040 °C for different time: (a) 5 h; (b) 8 h; (c) 12 h; (d) 15 h; (e) 18 h; (f) 20 h

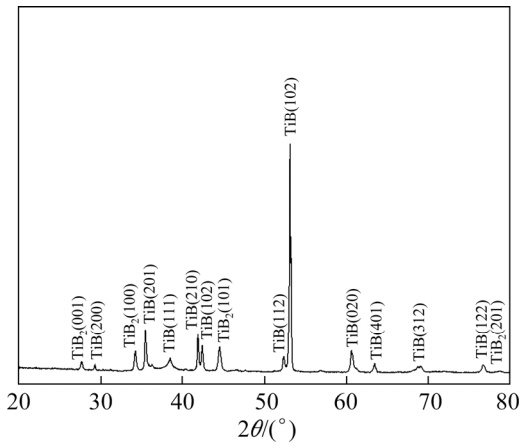

Fig. 4 XRD pattern of Ti−6Al−2Zr−1Mo−1V alloy borided at 1040 °C for 20 h

conditions, the boride layer thickness of the alloy was remarkably changed. The relatively thin boride layers of the alloy were predominant at 920 °C, and almost no TiB_2 layer occurred. As shown in Fig. 5, when the temperature was higher than 960 °C, boride layers with a continuous TiB_2 layer and TiB whiskers were obtained. In particular, thicker and more compact boride layers were achieved in the temperature range of 1000−1080 °C; as a result, the TiB_2 and TiB layers were approximately 6.1 and 35.7 μm thick, respectively, at 1080 °C. Spalling of the local boride layer was observed when the temperature exceeded 1120 °C, which resulted in a uniformly thick boride layer (see the arrow in

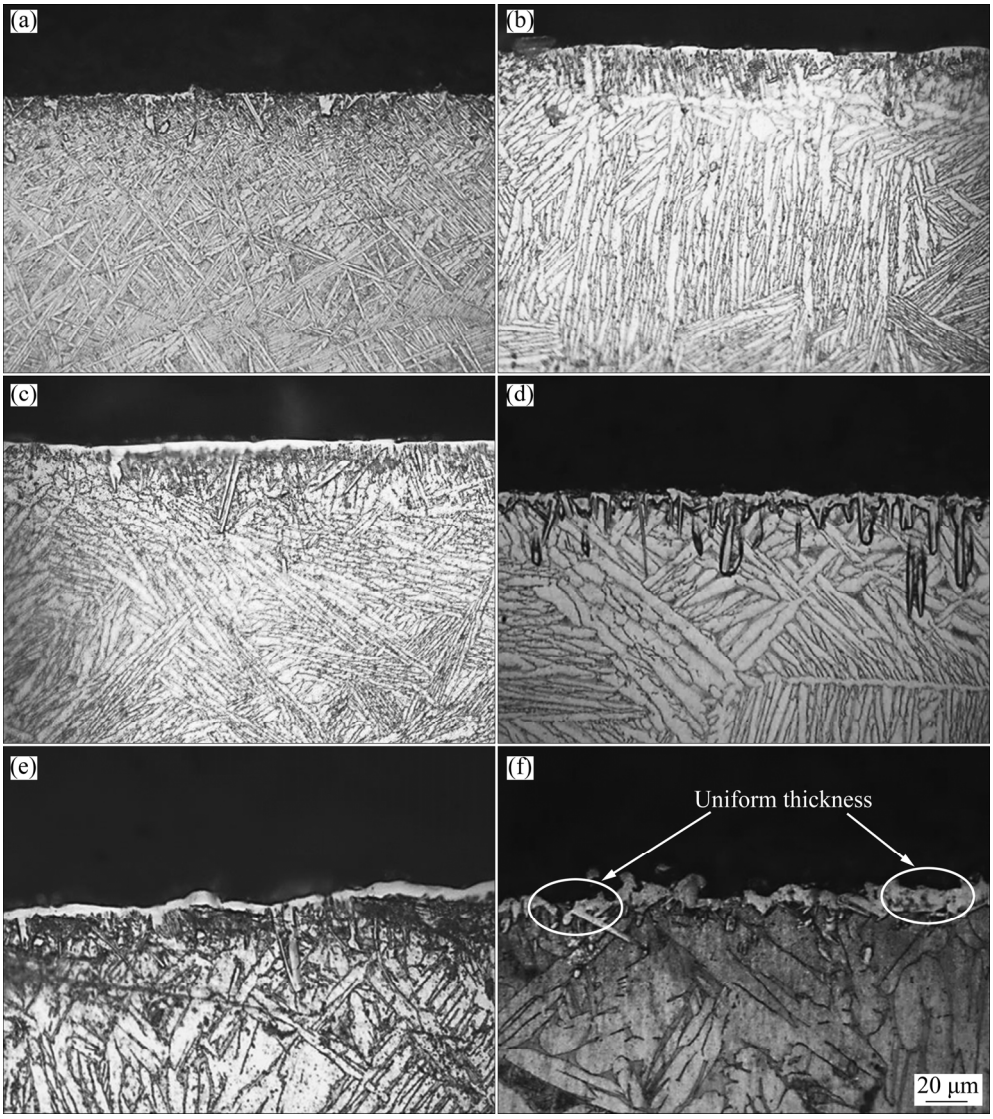

Fig. 5 Cross-sectional micrographs of boride layer of alloy borided at different temperatures for 20 h: (a) 920 °C; (b) 960 °C; (c) 1000 °C; (d) 1040 °C; (e) 1080 °C; (f) 1120 °C

Fig. 5(f)). The uniform borided layers will affect the wear resistance and service life.

The relationships between the boride layer thickness and the treatment time of the alloy borided in the temperature range of 920−1080 °C are plotted as boriding kinetics in Fig. 6. The boriding kinetic curves are considered S-shaped. With increasing treatment time, the boride layer thickness slowly increases before 5 h, subsequently rapidly increases in 5−15 h and finally slowly increases again after 15 h. As anticipated, with increasing boriding temperature, the boride layer thickens.

3.2 Modeling of layer growth kinetics

A diffusion-based model that describes the boride layer growth kinetics was constructed to predict the thickness development of the boride layers of Ti−6Al−2Zr−1Mo−1V alloy, as shown in Fig. 7. To simplify the proposed model in this work, four assumptions were made: (1) The boride layer is thin compared to the sample size, and the sample temperature is uniform throughout the boriding process. (2) The growth kinetics of the TiB_2 and TiB layers are only dominated by the diffusion-controlled mechanism. (3) The effect of the Ti matrix diffusion on the layer growth is ignored. (4) The diffusion coefficient of boron is independent of the concentration in the TiB_2 and TiB layers.

As an important steady diffusion law, diffusion balance equations were utilized to describe the

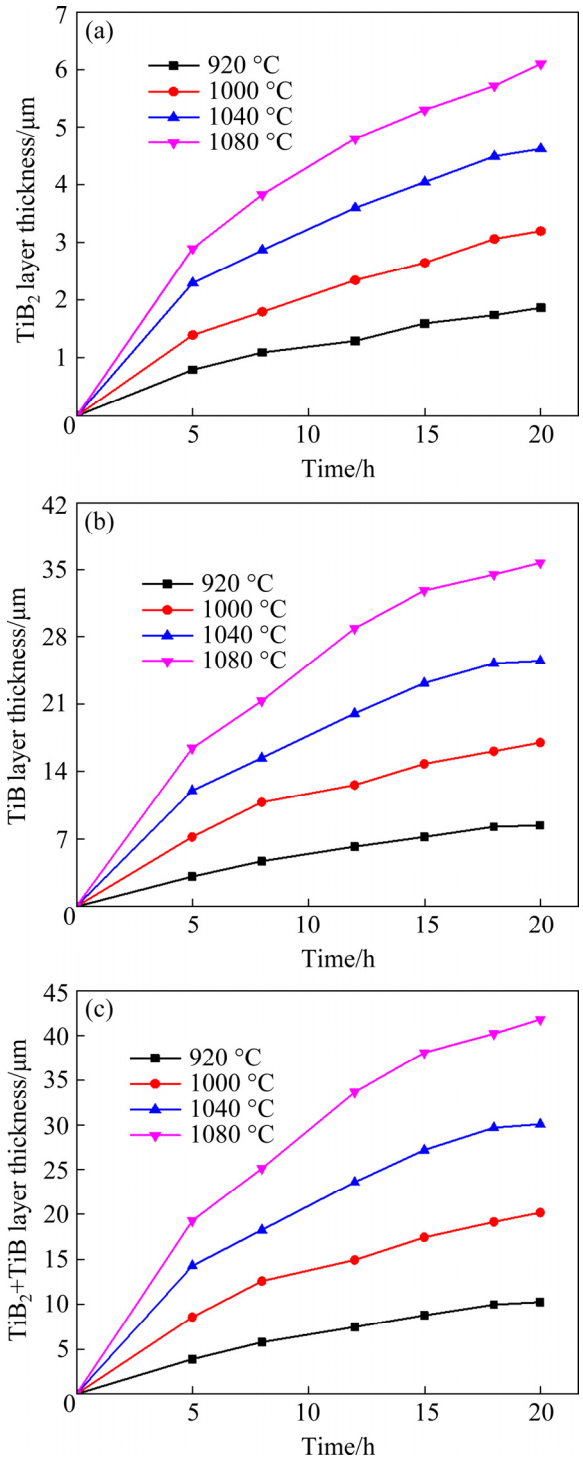

Fig. 6 Increase in boride layer thickness in relation to temperature and time of boriding treatment for TiB_2 layer (a), TiB layer (b) and TiB_2+TiB layer (c)

changes in boron concentration with time and location during the boriding process as follows [21]:

$$w_{\mathrm{TiB_2}}\frac{\mathrm{d}u}{\mathrm{d}t}=D_{\mathrm{B}}^{\mathrm{TiB_2}}\frac{C_{\mathrm{up}}^{\mathrm{TiB}}-C_{\mathrm{low}}^{\mathrm{TiB_2}}}{u}-D_{\mathrm{B}}^{\mathrm{TiB}}\frac{C_{\mathrm{up}}^{\mathrm{TiB}}-C_{\mathrm{low}}^{\mathrm{TiB}}}{v-u} \tag{1}$$

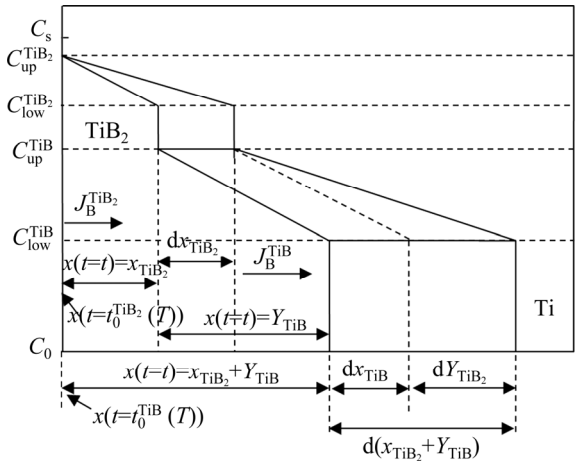

Fig. 7 Schematic representation of boron concentration through growth of (TiB_2/TiB) bilayer on substrate

$$w_{\mathrm{TiB}}\frac{\mathrm{d}v}{\mathrm{d}t}+w'\frac{\mathrm{d}u}{\mathrm{d}t}=D_{\mathrm{B}}^{\mathrm{TiB}}\frac{C_{\mathrm{up}}^{\mathrm{TiB}}-C_{\mathrm{low}}^{\mathrm{TiB}}}{v-u} \tag{2}$$

where

$$w_{\mathrm{TiB_2}}=[0.5(C_{\mathrm{up}}^{\mathrm{TiB_2}}-C_{\mathrm{low}}^{\mathrm{TiB_2}})+(C_{\mathrm{low}}^{\mathrm{TiB_2}}-C_{\mathrm{up}}^{\mathrm{TiB}})],$$

$$w_{\mathrm{TiB}}=[0.5(C_{\mathrm{up}}^{\mathrm{TiB}}-C_{\mathrm{low}}^{\mathrm{TiB}})+(C_{\mathrm{low}}^{\mathrm{TiB}}-C_0)],$$

$$w'=0.5\times(C_{\mathrm{up}}^{\mathrm{TiB}}-C_{\mathrm{low}}^{\mathrm{TiB}}),$$

$D_{\mathrm{B}}^{\mathrm{TiB_2}}$ and $D_{\mathrm{B}}^{\mathrm{TiB}}$ are the boron diffusion coefficients in the TiB_2 and TiB layers, respectively, and u and v are the thicknesses of TiB_2 layer and TiB+TiB_2 layer, respectively. Supposing that the thicknesses of TiB_2 layer and TiB layer follow parabolic growth, the TiB_2 and TiB layer thicknesses can be expressed as

$$u=k_1t^{0.5} \tag{3}$$

$$v=k_2t^{0.5} \tag{4}$$

$$l=(k_2-k_1)t^{0.5} \tag{5}$$

where l is the TiB layer thickness; k_1 and k_2 are the parabolic growth constants at the TiB_2/TiB interface and TiB/Ti interface, respectively, which are determined by the relationship of u–$t^{0.5}$ and v–$t^{0.5}$ (as shown in Fig. 8). Substituting Eqs. (3) and (4) into Eqs. (1) and (2) and introducing the correcting factors A for $D_{\mathrm{B}}^{\mathrm{TiB_2}}$ and B for $D_{\mathrm{B}}^{\mathrm{TiB_2}}$, we have

$$D_{\mathrm{B}}^{\mathrm{TiB_2}}=A\frac{(w_{\mathrm{TiB_2}}+w')k_1^2+w_{\mathrm{TiB}}k_1k_2}{2(C_{\mathrm{up}}^{\mathrm{TiB_2}}-C_{\mathrm{low}}^{\mathrm{TiB_2}})} \tag{6}$$

$$D_{\mathrm{B}}^{\mathrm{TiB}}=B\frac{(w'k_1+w_{\mathrm{TiB}}k_2)(k_2-k_1)}{2(C_{\mathrm{up}}^{\mathrm{TiB}}-C_{\mathrm{low}}^{\mathrm{TiB}})} \tag{7}$$

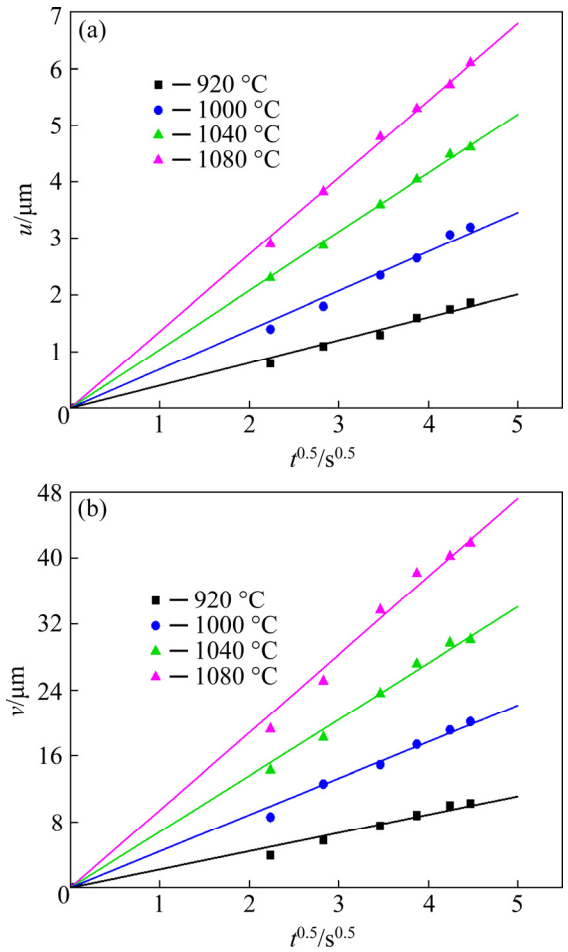

Fig. 8 Plots of boride layer thickness vs square root of boriding time: (a) TiB_2 layer; (b) TiB_2+TiB layer

To determine $D_B^{TiB_2}$ and D_B^{TiB}, the initial and boundary conditions of the boron diffusion problem were set up as $C(x, 0)=0$, $C_{up}^{TiB_2}=31.1\%$, $C_{low}^{TiB_2}=30.1\%$, $C_{up}^{TiB}=18.5\%$, and $C_{low}^{TiB}=18\%$. Since the diffusion models of $d^2=Dt$ and $d=kt^{0.5}$ can describe the growth kinetics of the boride layer at identical temperature, the correcting factors A of 0.0146 and B of 0.0467 were determined as follows:

$$A=k_1^2 / \frac{(w_{TiB_2}+w')k_1^2+w_{TiB}k_1k_2}{2(C_{up}^{TiB_2}-C_{low}^{TiB_2})} \quad (8)$$

$$B=(k_2-k_1)^2 / \frac{(w_{TiB_2}+w')k_1^2+w_{TiB}k_1k_2}{2(C_{up}^{TiB_2}-C_{low}^{TiB_2})} \quad (9)$$

As a result, boron diffusion coefficients, $D_B^{TiB_2}$ and D_B^{TiB}, can be obtained according to Eq. (6) and Eq. (7), respectively. The values of $D_B^{TiB_2}$ and D_B^{TiB} are listed in Table 1. Generally, diffusion coefficient D for the boriding process related to the boriding temperature can be described by an Arrhenius-type expression:

$$D=D_0\exp[-Q/(RT)] \quad (10)$$

where D_0 is the pre-exponential factor (m^2/s), Q is the activation energy (J/mol), R is the gas constant (kJ/(mol·K)), and T is the boriding temperature (K).

Taking natural logarithms on both sides of Eq. (7), we have

$$\ln D=\ln D_0-Q/(RT) \quad (11)$$

Figure 9 shows the linear relationship of $D_B^{TiB_2}-1/T$ and $D_B^{TiB}-1/T$ for TiB_2 and TiB, where the values of $D_B^{TiB_2}$ and D_B^{TiB} are determined from Table 1. The values of $-Q^{TiB_2}/R$ and $-Q^{TiB}/R$ are equal to the linear slope of the curves of $D^{TiB_2}-1/T$ and $D^{TiB}-1/T$, respectively. The values of $\ln D_0^{TiB_2}$ and $\ln D_0^{TiB}$ are equal to the linear intercept of the curves of $D^{TiB_2}-1/T$ and $D^{TiB}-1/T$, respectively. As a result, the following equations for the diffusion coefficients $D_B^{TiB_2}$ and D_B^{TiB} are obtained:

$$D_B^{TiB_2}=2.07\times10^{-7}\exp(-\frac{223.1}{RT}) \quad (12)$$

$$D_B^{TiB}=5.99\times10^{-5}\exp(-\frac{246.9}{RT}) \quad (13)$$

Consequently, the TiB_2 layer thickness d_{TiB_2}, TiB layer thickness d_{TiB} and TiB_2+TiB layer thickness d_{TiB_2+TiB} can be calculated according to Eqs. (14)−(16), respectively. The boron activation energies in the TiB_2 layer and TiB layer were determined to be 223.1 kJ/mol and 246.9 kJ/mol,

Table 1 Parabolic growth constants at TiB_2/TiB and TiB/Ti interfaces and diffusion coefficients at different temperatures

T/°C	k_1/(μm·s$^{-0.5}$)	k_2/(μm·s$^{-0.5}$)	(k_2-k_1)/(μm·s$^{-0.5}$)	$D_B^{TiB_2}$/(m·s^{-1})	D_B^{TiB}/(m·s^{-1})
920	0.0067	0.0371	0.0304	3.72×10^{-17}	9.64×10^{-16}
1000	0.0115	0.0739	0.0624	1.25×10^{-16}	3.94×10^{-15}
1040	0.0173	0.1135	0.0962	2.89×10^{-16}	9.33×10^{-15}
1080	0.0227	0.1572	0.1345	5.22×10^{-16}	1.81×10^{-14}

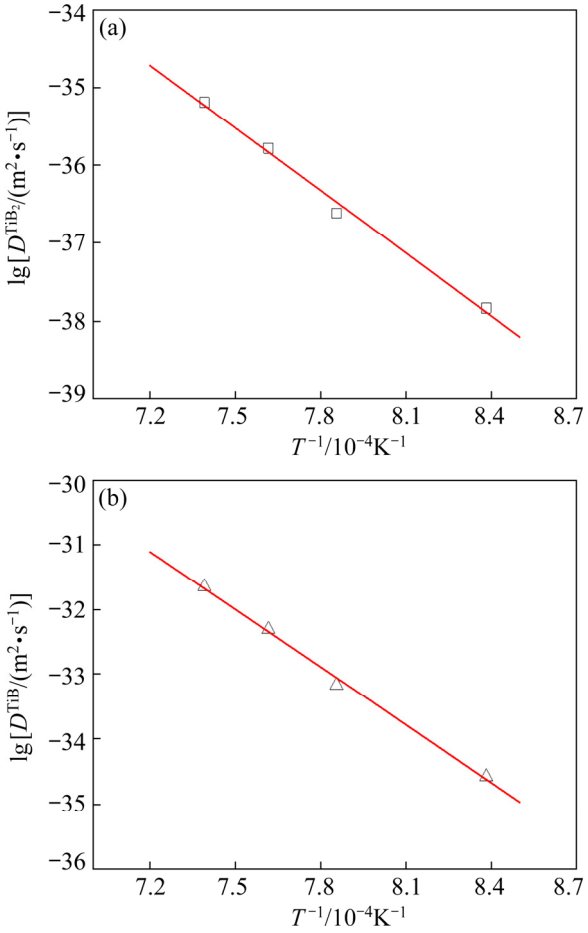

Fig. 9 Linear relationship of $D^{TiB_2}-1/T$ (a) and $D^{TiB}-1/T$ (b)

respectively, in the present work. The boron activation energy for the present Ti alloy is higher than that for several titanium alloys, such as Ti6Al4V alloy reported by KEDDAM and TAKTAK [12] and Ti−45Nb alloy reported by KARA and PURCEK [13].

$$d_{TiB_2}^2 = D_B^{TiB_2} t \tag{14}$$

$$d_{TiB}^2 = D_B^{TiB} t \tag{15}$$

$$d_{TiB_2+TiB} = d_{TiB_2} + d_{TiB} \tag{16}$$

Figure 10 shows the calculated and experimental values of the TiB_2 layer, TiB layer and TiB_2+TiB layer thickness of the alloy borided at 920−1080 °C for 5−20 h. There is satisfactory consistency between experimental data and model prediction. Hence, the present model can be considered a prediction of the growth kinetics of the boriding layers for Ti−6Al−2Zr−1Mo−1V alloy.

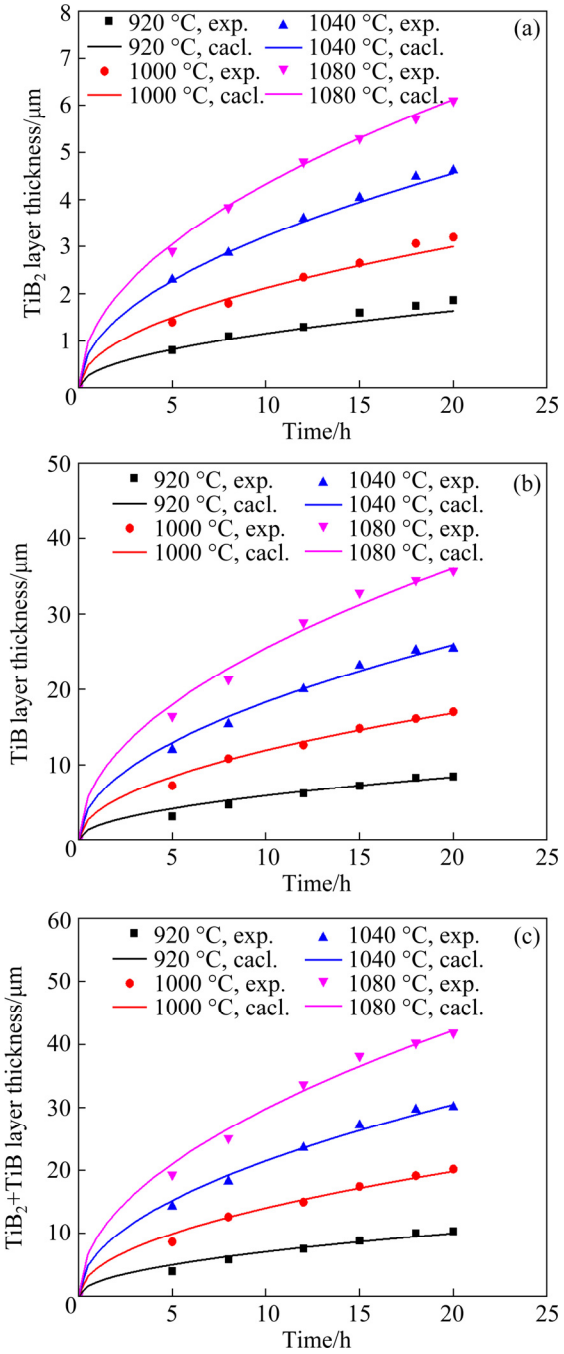

Fig. 10 Comparison of calculated and experimental values of TiB_2 layer thickness (a), TiB layer thickness (b) and TiB_2+TiB layer thickness (c)

4 Conclusions

(1) The formation of TiB_2 and TiB layers has a predominant sawtooth-like morphology. The outer boride layer only includes the TiB_2 phase, and the TiB phase appears below the outer layer.

(2) The boride layer depth increases with the boriding temperature and time. The boride layer

growth kinetics is characterized by a parabolic curve.

(3) Thick and compact boride layers were obtained when the boriding temperatures were 1000−1080 °C and the treatment time exceeded 8 h.

(4) The boron activation energies were determined to be 223.1 and 246.9 kJ/mol in TiB_2 layer and TiB layer, respectively.

(5) The growth kinetics of the boride layers, including both TiB_2 and TiB layers, was predicted by establishing a diffusion model, which was satisfactorily consistent with the experimental data.

Acknowledgments

The authors are grateful for the financial supports from the National Natural Science Foundation of China (Nos. 51761029, 51864035), the Natural Science Foundation of Jiangxi Province, China (Nos. 2020BABL204011 and 2020BABL204007), and Key Laboratory for Microstructural Control of Metallic Materials of Jiangxi Province (Nanchang Hangkong University), China (Nos. EJ201701513 and EJ201901454).

References

[1] LEI Z N, GAO P F, LI H W, CAI Y, ZHAN M. On the fracture behavior and toughness of TA15 titanium alloy with tri-modal microstructure [J]. Materials Science and Engineering A, 2019, 753: 238−246.

[2] ZHAO Hui-jun, WANG Bao-yu, JU Dong-ying, CHEN Guo-jin. Hot tensile deformation behavior and globularization mechanism of bimodal microstructured Ti−6Al−2Zr−1Mo−1V alloy [J]. Transactions of Nonferrous Metals Society of China, 2018, 28(12): 2449−2459.

[3] ZHAO J, WANG K H, LV L X, LIU G. Evolution and distribution of geometrically necessary dislocations for TA15 titanium alloy sheets during the hot tensile process [J]. The Journal of the Minerals Metals & Materials Society, 2019, 71(7): 1−10.

[4] DU Yu-xuan, YANG Xin-liang, LI Zu-shu, HAO Fang, MAO You-chuan, LI Shao-qiang, LIU Xiang-hong, FENG Yong, YAN Zhi-ming. Shear localization behavior in hat-shaped specimen of near-α Ti6Al2Zr1Mo1V titanium alloy loaded at high strain rate [J]. Transactions of Nonferrous Metals Society of China, 2021, 31(6): 1641−1655.

[5] TIAN Y S, ZHANG Q Y, WANG D Y. Study on the microstructures and properties of the boride layers laser fabricated on Ti–6Al–4V alloy [J]. Journal of Materials Processing Technology, 2009, 209(6): 2887−2891.

[6] TÜRKMEN İ, YALAMAÇ E. Growth of the Fe_2B layer on SAE 1020 steel employed a boron source of H_3BO_3 during the powder-pack boriding method [J]. Journal of Alloys and Compounds, 2018, 744: 658−666.

[7] MAKUCH N, KULKA M, DZIARSKI P, TAKTAK S. The influence of chemical composition of Ni-based alloys on microstructure and mechanical properties of plasma paste borided layers [J]. Surface and Coatings Technology, 2019, 367: 187−202.

[8] PERETTI V, FERRARIS S, GAUTIER G, HELLMICH C, LAHAYNE O, STELLA B, YAMAGUCHI S, SPRIANO S. Surface treatments for boriding of Ti6Al4V alloy in view of applications as a biomaterial [J]. Tribology International, 2018, 126: 21−28.

[9] KAOUKA A, BENAROUS K. Electrochemical boriding of titanium alloy Ti−6Al−4V [J]. Journal of Materials Research and Technology, 2019, 8(6): 6407−6412.

[10] SARMA B, TIKEKAR N M, RAVI CHANDRAN K S. Kinetics of growth of superhard boride layers during solid state diffusion of boron into titanium [J]. Ceramics International, 2012, 38(8): 6795−6805.

[11] LI P, LIU D, BAO W Z, MA L, DUAN Y H. Surface characterization and diffusion model of pack borided TB_2 titanium alloy [J]. Ceramics International, 2018, 44(15): 18429−18437.

[12] KEDDAM M, TAKTAK S. Characterization and diffusion model for the titanium boride layers formed on the Ti6Al4V alloy by plasma paste boriding [J]. Applied Surface Science, 2017, 399: 229−236.

[13] KARA G, PURCEK G. Growth kinetics and mechanical characterization of boride layers formed on β-type Ti−45Nb alloy [J]. Surface and Coatings Technology, 2018, 352: 201−212.

[14] LIU D, DUAN Y H, BAO W Z, PENG M J. Characterization and growth kinetics of boride layers on Ti−5Mo−5V−8Cr−3Al alloy by pack boriding with CeO_2 [J]. Materials Characterization, 2020, 164: 110362.

[15] CHEN T, KOYAMA S. Influence of boriding temperature on microstructure and tribological properties of titanium [J]. Solid State Sciences, 2020, 107: 106369.

[16] DUAN Y H, WANG X Y, LIU D, BAO W Z, LI P, PENG M J. Characteristics, wear and corrosion properties of borided pure titanium by pack boriding near $\alpha \rightarrow \beta$ phase transition temperature [J]. Ceramics International, 2020, 46(10): 16380−16387.

[17] PENG M J, DUAN Y H, MA L S, SHU B P. Characteristics of surface layers on Ti6Al4V alloy borided with CeO_2 near the transition temperature [J]. Journal of Alloys & Compounds, 2018, 769: 1−9.

[18] LV X J, HU L Y, SHUANG Y J, LIU J H, LAI Y Q, JIANG L X, LI J. The growth behavior of titanium boride layers in α and β phase fields of titanium [J]. Metallurgical & Materials Transactions A, 2016, 47(7): 3573−3579.

[19] POPELA T, VOJTĚCH D. Characterization of pack-borided last-generation TiAl intermetallics [J]. Surface and Coatings Technology, 2012, 209: 90−96.

[20] DUAN Y H, LI P , CHEN Z Z, SHI J, MA L S. Surface evolution and growth kinetics of Ti6Al4V alloy in pack boriding [J]. Journal of Alloys & Compounds, 2018, 742: 690−701.

[21] KEDDAM M, KULKA M. A kinetic model for the boriding kinetics of AISI D2 steel during the diffusion annealing process [J]. Protection of Metals & Physical Chemistry of Surfaces, 2018, 54(2): 282−290.

Ti−6Al−2Zr−1Mo−1V 合金 TiB_2/TiB 渗硼层实验和模拟

欧阳德来[1]，胡圣伟[1]，陶 成[1]，崔 霞[1]，朱知寿[2]，鲁世强[1]

1. 南昌航空大学 江西省金属材料微结构调控重点实验室，南昌 330063；
2. 北京航空材料研究院，北京 100095

摘 要：对 Ti−6Al−2Zr−1Mo−1V 合金在 920~1120 °C 温度范围进行渗硼处理，研究渗硼条件对渗硼层的影响。结果表明，渗硼层由外部连续薄 TiB_2 层和里层厚 TiB 层组成，TiB 相呈魏氏体状或针状形貌嵌入基体。在渗硼温度为 1000~1080 °C、渗硼时间超过 8 h 渗硼时可获得厚而致密的渗硼层。渗硼层厚度随渗硼温度和渗硼时间增加而增加。渗硼层生长动力学曲线呈抛物线特征。建立 TiB_2 和 TiB 层生长动力学的预测模型，其计算结果与实验数据达到较好吻合。确定 TiB_2 和 TiB 激活能分别为 223.1 和 246.9 kJ/mol。

关键词：Ti−6Al−2Zr−1Mo−1V 合金；渗硼；显微组织；模型

(Edited by Bing YANG)